CDF/PHYS/JET/PUBLIC/10818
Draft v2.0

Measurement of the cross section for direct photon production in association with a heavy quark in $p\bar{p}$ collisions at $\sqrt{s} = 1.96$ TeV

The CDF Collaboration

November 2, 2012

Abstract

We report on a measurement of the cross section for direct photon production in association with a heavy quark (b or c) using a data sample of $p\bar{p}$ collisions at $\sqrt{s} = 1.96$ TeV collected by the CDF II detector at the Fermilab Tevatron, with an integrated luminosity of 9.1 fb^{-1}. Measurements are performed as a function of the photon transverse energy, covering photon transverse energy $30 < E_T^\gamma < 300$ GeV, photon rapidities $|y^\gamma| < 1.0$, jet transverse energy $E_T^{jet} > 20$ GeV, and jet rapidities $|y^{jet}| < 1.5$. The results are compared with several theoretical predictions.

The study of direct photon (γ) production in association with a heavy quark Q (b or c) in hadronic collisions provides valuable information on the parton distributions of the initial state hadrons. At photon transverse energies E_T^γ below 100 GeV, such events are produced predominantly by QCD Compton scattering process $gQ \to \gamma Q$, while above that value the dominant process is quark-antiquark annihilation with gluon splittings to heavy quarks $q\bar{q} \to \gamma g \to \gamma Q\bar{Q}$ [1]. A cross section measurement of $\gamma + Q + X$ production provides information on the b, c, and gluon densities within the colliding hadrons, and consequently place constraints on the b, c, and gluon parton distribution functions (PDFs) and the rate of gluon splitting to heavy quarks, which have substantial uncertainties.

The D0 Collaboration has measured the cross section of photons in association with heavy flavor jets using data collected at $\sqrt{s} = 1.96$ TeV, covering the range $30 < E_T^\gamma < 150$ GeV [2]. The rate for bottom quark jets agrees very well with a Next-to-leading order (NLO) perturbative QCD prediction [1]; however the corresponding charm jet cross section deviates strongly from the pQCD prediction for $E_T^\gamma > 70$ GeV. There has been an attempt to explain the photon plus charm jet discrepancy as a hint for an intrinsic contribution to the charm structure function [3]. However, the updated D0 measurements [4] show notable disagreement with the NLO pQCD prediction for $\gamma + b + X$ in the region $E_T^\gamma \gtrsim 70$ GeV with slightly different kinematic cuts. The CDF Collaboration has measured the process $p\bar{p} \to \gamma + b + X$ at $\sqrt{s} = 1.96$ TeV, employing a

photon and heavy flavor trigger to improve the low energy photon acceptance, covering the range $20 < E_T^\gamma < 70$ GeV [5]. The measured cross section agrees well with the NLO pQCD prediction. In this paper, we present the updated measurements of the cross sections for $p\bar{p} \to \gamma + b + X$ and $p\bar{p} \to \gamma + c + X$ processes, using the full dataset of 9.1 fb^{-1} of integrated luminosity collected by the CDF II detector at the Fermilab Tevatron using $p\bar{p}$ collisions at $\sqrt{s} = 1.96$ TeV, exploring E_T^γ up to 300 GeV.

The CDF II detector has a cylindrical geometry with approximate forward-backward and azimuthal symmetry. It consists of a tracking system in a 1.4 T magnetic field, coaxial with the beam, surrounded by calorimeters and muon detection chambers [6]. The tracking system consists of a silicon tracker (SVX-II) [7] and an open cell drift chamber (COT) [8]. The fiducial region of the silicon detector covers the pseudorapidity range $|\eta| < 2.0$ [6]; this subsystem, the closest to the beam-pipe and with the finest segmentation, is used for reconstructing displaced vertices from heavy flavor decays. The drift chamber measures the momentum of charged particles in the region $|\eta| < 1.0$. The central and plug calorimeters [9] are sampling calorimeters that surround the COT and cover the range $|\eta| < 1.1$ and $1.2 < |\eta| < 3.6$, respectively. The calorimeters, consisting of electromagnetic (EM) and hadronic layers arranged in a projective geometry, allow measurement of the "transverse energy" $E_T = E\sin(\theta)$ [6]. At the approximate electromagnetic shower maximum, the EM calorimeters contain fine-grained detectors (central electromagnetic strip chambers - CES) [10] that measure the shower shape and centroid position in the two dimensions transverse to the shower development. Surrounding these detectors is a system of muon detectors [11].

The data are collected using a three-level online event selection system that selects events with at least one energy cluster consistent with a photon in the final state. Photons are collected with two trigger thresholds in E_T^γ, 25 GeV and 70 GeV. In order to reduce contamination from neutral meson decays, the low E_T^γ trigger requires photon clusters to be isolated. The low E_T^γ trigger also requires the lateral shower profile of the CES cluster to be consistent with that of electrons, as measured in test beam data. The combination of the two triggers is measured to be effectively 100% efficient for the kinematic region used in this measurement.

The event selection requires the primary vertex z position to be within 60 cm of the center of the detector. In order to suppress beam-related backgrounds, cosmic rays, and calorimeter noise, the missing transverse energy of the event has to be less than 80% of the transverse energy of the leading photon candidate. In the selected sample, each event is required to have at least one photon candidate and one jet identified as a heavy flavor jet. The photon candidate is required to be in the fiducial region of the central calorimeter (approximately in the region $|\eta| < 1.04$). The transverse energy of the photon is corrected to account for nonuniformities in the calorimeter response, and calibrated using electrons from reconstructed Z bosons. Photon candidates are required to have $E_T^\gamma > 30$ GeV and satisfy loose selection requirements, as described in Ref. [12]. After additional track requirements are applied to remove electrons, an artificial neural network (ANN) technique is constructed from several detector variables mostly employing information in the EM and hadronic calorimeters to further reduce

background [13]. The photon candidates are required to have an ANN output value above 0.75.

At least one jet must be present in each event. Jets are reconstructed using the JETCLU algorithm [14] with a cone radius $R = \sqrt{(\Delta\phi)^2 + (\Delta\eta)^2} = 0.4$ [6]. To recover the true hadronic energy, jets are corrected for instrumental effects [15]. We only select jets that have $E_T > 20$ GeV within $|\eta| < 1.5$. At least one jet is classified as a heavy flavor jet using a secondary vertex tagger [16]. This tagging algorithm exploits the long lifetime of the b/c-hadrons, and is based on the reconstruction of a displaced, or secondary, vertex using the reconstructed charged particle tracks, contained within a cone of 0.4 around the jet axis. The secondary vertex must be more than 2 standard deviations away from the beam position, in the same direction as the jet momentum. If there are multiple tagged jets in the kinematic region, the one with the highest E_T is selected. The selected jet is then required to lie outside a cone of 0.4 surrounding the photon candidate. The efficiency of the tagging algorithm is 25% for taggable b jets of $E_T = 20$ GeV and increases to 40% for $E_T \gtrsim 50$ GeV and less for c jets.

After all the selection requirements, 214 336 events remain in the data samples. In these events there are two background sources: jets faking photons and light flavor jets faking heavy flavor jets. To estimate the rate of fake photons, the photon ANN distribution in data is fitted to a linear combination of templates for photons and jets obtained from simulated inclusive photon sample and dijet sample after applying all the photon selection cuts except the cut on the ANN output. Events with photons produced from initial state radiation (ISR) or final state radiation (FSR) are removed from the dijet sample since they are prompt photons and should be considered as signal events. The remaining events are predominantly π^0's and η's. A fit is performed in each E_T^γ bin, yielding photon purities between 77% and 94% for events with ANN output value above 0.75. The obtained photon purities and one example fit are shown in Fig. 1. The systematic uncertainties on the photon purities are estimated by varying the input variables to the Photon ID ANN within their uncertainties. The dominant error originates from the uncertainties in the modeling of calorimeter isolation energy. The total uncertainty is estimated to decrease from 6% at $E_T^\gamma = 30$ GeV to 2% for $E_T^\gamma > 70$ GeV.

Backgrounds to heavy flavor jets arise from light flavor jets where random combinations of tracks mimic a displaced vertex. The fractions of b- and c-jets are determined from fitting the invariant mass of tracks associated with the secondary vertex (M_{SecVtx}) using simulated templates of the shapes expected for b-, c-, and light-quark jets. The shape of fake photon background is modeled using dijet data where one jet is required to deposit most of energy in the EM calorimeter to mimic a photon and the other jet is required to pass all the heavy flavor jet selection cuts. This background component is then constrained to the measured fake photon rate from the fit of photon ID ANN output distribution. Figure 2 shows the result of the fit for photons with $40 < E_T^\gamma < 50$ GeV, as an example. The b-jet fractions vary between 22% and 37% and the c-jet fractions vary between 16% and 42% for the tagged jets, after subtracting the contribution of fake photon background. The total systematic uncertainties range between

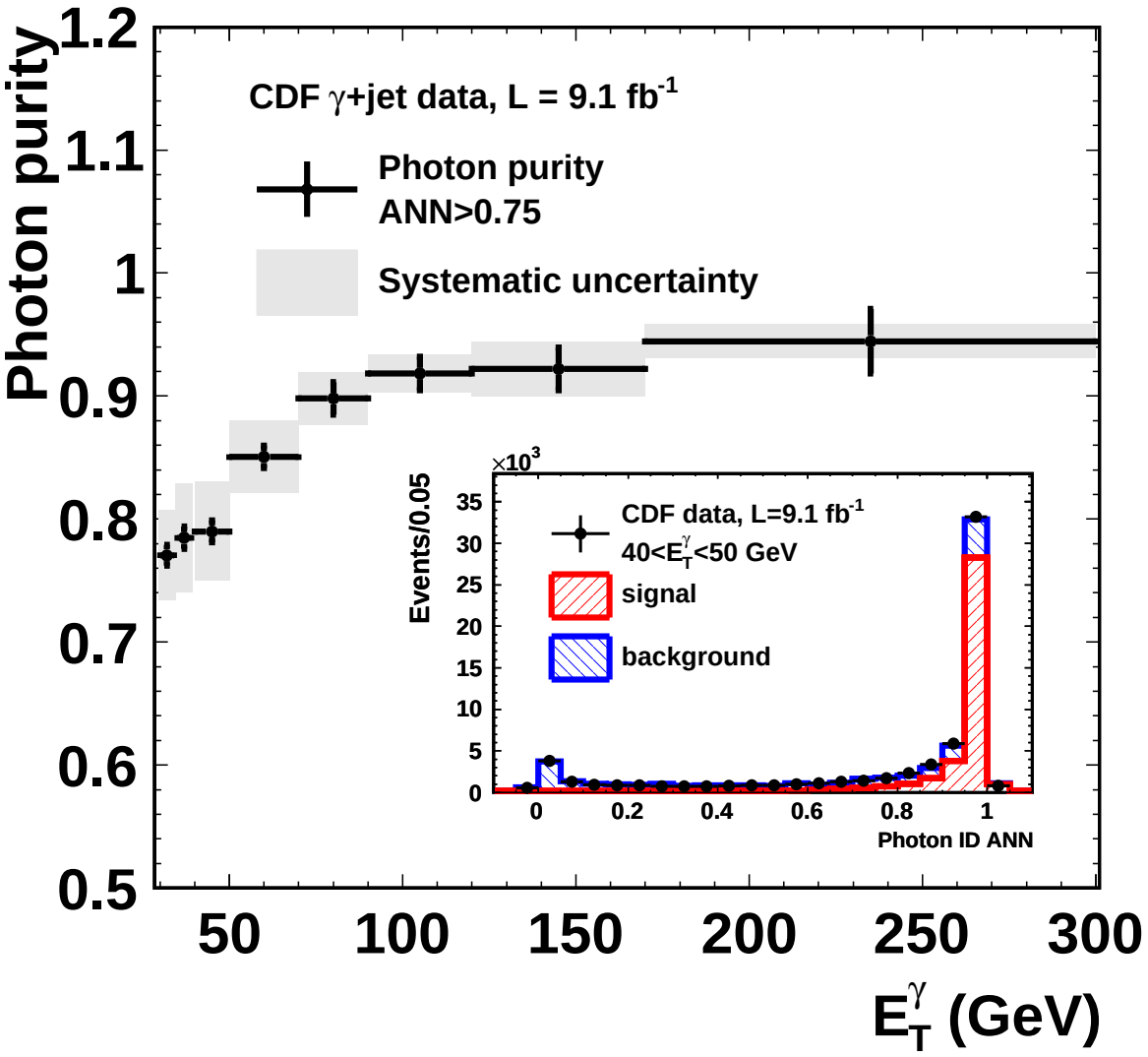

Figure 1: Photon purity as a function of E_T^γ in the selected data sample. Embedded is the fit for photon candidates with $40 < E_T^\gamma < 50$ GeV.

15-30% and are dominated by the uncertainties in the simulated M_{SecVtx} template shapes originated from the mismodeling of tracking efficiency in the tracking system.

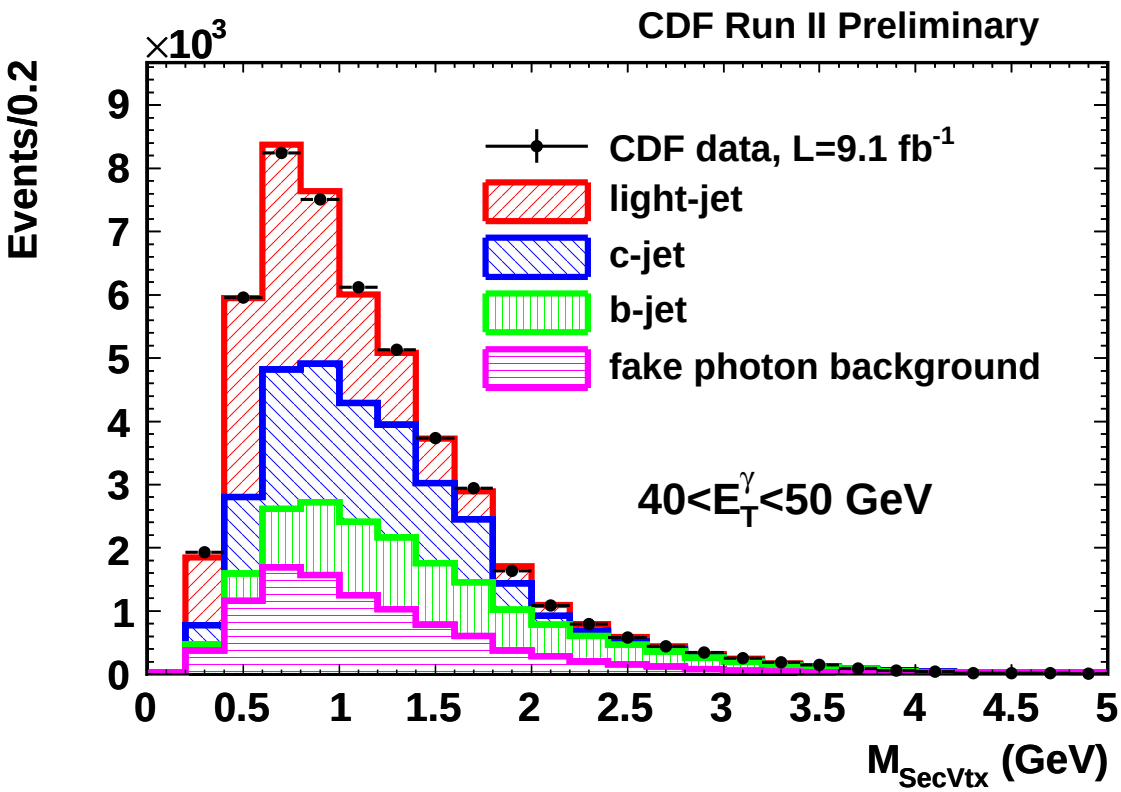

Figure 2: Distribution of the secondary vertex mass of tagged jets after applying all selection cuts, for photon candidates with $40 < E_T^\gamma < 50$ GeV. The points are data, and the stacked, shaded histograms represent the estimated contributions of the b-, c-, and light-quark jets from the fit and fake photon background.

The raw differential cross section as a function of E_T^γ is defined as $d\sigma^{b/c}/dE_T^\gamma = Nf_\gamma f_{b/c}/(\Delta E_T^\gamma \epsilon_{\rm trig}\mathcal{L})$, where N is the number of data events in a given E_T^γ bin after applying all the selections, f_γ is the photon purity, $f_{b/c}$ is the b-jet/c-jet fraction, ΔE_T^γ is the size of the E_T^γ bin, $\epsilon_{\rm trig}$ is the trigger efficiency, and $\mathcal{L}$ is the integrated luminosity. The trigger efficiency is approximately 100% in the kinematic region of the measurement. The measured cross section is corrected for acceptance, efficiencies of the photon selection and tagging algorithm and resolution effects back to the hadron level using a bin-by-bin unfolding procedure and a sample of prompt-photon events simulated with SHERPA 1.4.1 [18]. The photon efficiency is calibrated by comparing the efficiencies of selecting data and simulated $Z^0 \to e^+e^-$ events. The tagging efficiency is calibrated to heavy flavor jets enriched data. The unfolding factors range from 18% to 27% for $\gamma + b + X$ events and from 4% to 8% for $\gamma + c + X$ events. The total systematic uncertainties are estimated to be approximately 10% and are dominated by

the uncertainties in photon energy scale and tagging efficiency.

The differential cross sections of $\gamma+b+X$ and $\gamma+c+X$ productions are extracted in eight bins of E_T^γ, and are listed in Table 1. The results are also shown in Fig. 3 as a function of E_T^γ. The total systematic uncertainties range between 18-35% and are dominated by the systematics of the b-jet/c-jet fractions fits.

Table 1: The $\gamma+b+X$ and $\gamma+c+X$ cross sections in bins of E_T^γ together with statistical and systematic uncertainties. Four theoretical predictions are shown. The last column shows non-perturbative corrections applied to the NLO and k_T-factorization parton level predictions.

E_T^γ bins (GeV)	$\frac{d\sigma}{dE_T^\gamma}$ (pb/GeV)	NLO (pb/GeV)	k_T frac. (pb/GeV)	SHERPA (pb/GeV)	PYTHIA (pb/GeV)	Corr.
			$\gamma+b+X$			
30-35	1.47±0.07±0.41	2.09	1.76	1.84	1.09	0.937
35-40	$(8.90\pm0.49\pm2.49)\times10^{-1}$	1.16	1.05	1.16	7.38×10^{-1}	0.936
40-50	$(4.87\pm0.25\pm1.26)\times10^{-1}$	5.18×10^{-1}	4.89×10^{-1}	6.04×10^{-1}	3.44×10^{-1}	0.915
50-70	$(1.60\pm0.09\pm0.40)\times10^{-1}$	1.53×10^{-1}	1.60×10^{-1}	2.08×10^{-1}	1.02×10^{-1}	0.966
70-90	$(5.17\pm0.51\pm1.41)\times10^{-2}$	3.59×10^{-2}	4.24×10^{-2}	5.83×10^{-2}	2.94×10^{-2}	0.954
90-120	$(1.79\pm0.18\pm0.50)\times10^{-2}$	9.45×10^{-3}	1.25×10^{-2}	1.79×10^{-2}	8.22×10^{-3}	0.920
120-170	$(4.49\pm0.81\pm1.58)\times10^{-3}$	1.98×10^{-3}	3.13×10^{-3}	4.19×10^{-3}	1.94×10^{-3}	0.907
170-300	$(6.39\pm2.26\pm2.04)\times10^{-4}$	1.90×10^{-4}	3.99×10^{-4}	4.30×10^{-4}	2.37×10^{-4}	0.913
			$\gamma+c+X$			
30-35	$(1.16\pm0.05\pm0.20)\times10$	1.74×10	1.07×10	1.25×10	8.01	1.28
35-40	6.33±0.33±1.08	8.82	6.22	7.23	4.39	1.25
40-50	2.92±0.17±0.48	3.67	2.65	3.43	2.01	1.21
50-70	$(7.62\pm0.60\pm1.39)\times10^{-1}$	8.54×10^{-1}	7.26×10^{-1}	9.79×10^{-1}	5.12×10^{-1}	1.16
70-90	$(1.67\pm0.35\pm0.37)\times10^{-1}$	1.62×10^{-1}	1.71×10^{-1}	2.28×10^{-1}	1.05×10^{-1}	1.13
90-120	$(4.37\pm1.44\pm0.85)\times10^{-2}$	3.51×10^{-2}	4.99×10^{-2}	5.90×10^{-2}	2.50×10^{-2}	1.11
120-170	$(1.32\pm0.55\pm0.26)\times10^{-2}$	5.44×10^{-3}	1.25×10^{-2}	1.20×10^{-2}	4.56×10^{-3}	1.07
170-300	$(1.51\pm1.23\pm0.45)\times10^{-3}$	3.86×10^{-4}	1.92×10^{-3}	1.12×10^{-3}	4.84×10^{-4}	1.04

NLO pQCD predictions [1] are given in Table 1 and shown in Fig. 3. These predictions include pointlike photon subprocesses through $\mathcal{O}(\alpha\alpha_s^2)$ and fragmentation subprocesses through $\mathcal{O}(\alpha_s^3)$. The calculation is performed using a phase space slicing technique so that the effects of experimental cuts can be included. CTEQ6.6M PDFs are utilized in the calculation. The scale dependence is evaluated by varying the renormalization, μ_r, factorization, μ_f and fragmentation, μ_F scales from the default value p_T^γ to $p_T^\gamma/2$ and $2p_T^\gamma$.

The predictions based on a k_T-factorization approach [20] are reported in Table 1 and Fig. 3. This calculation is based on $\mathcal{O}(\alpha\alpha_s^2)$ off-shell amplitudes of gluon-gluon

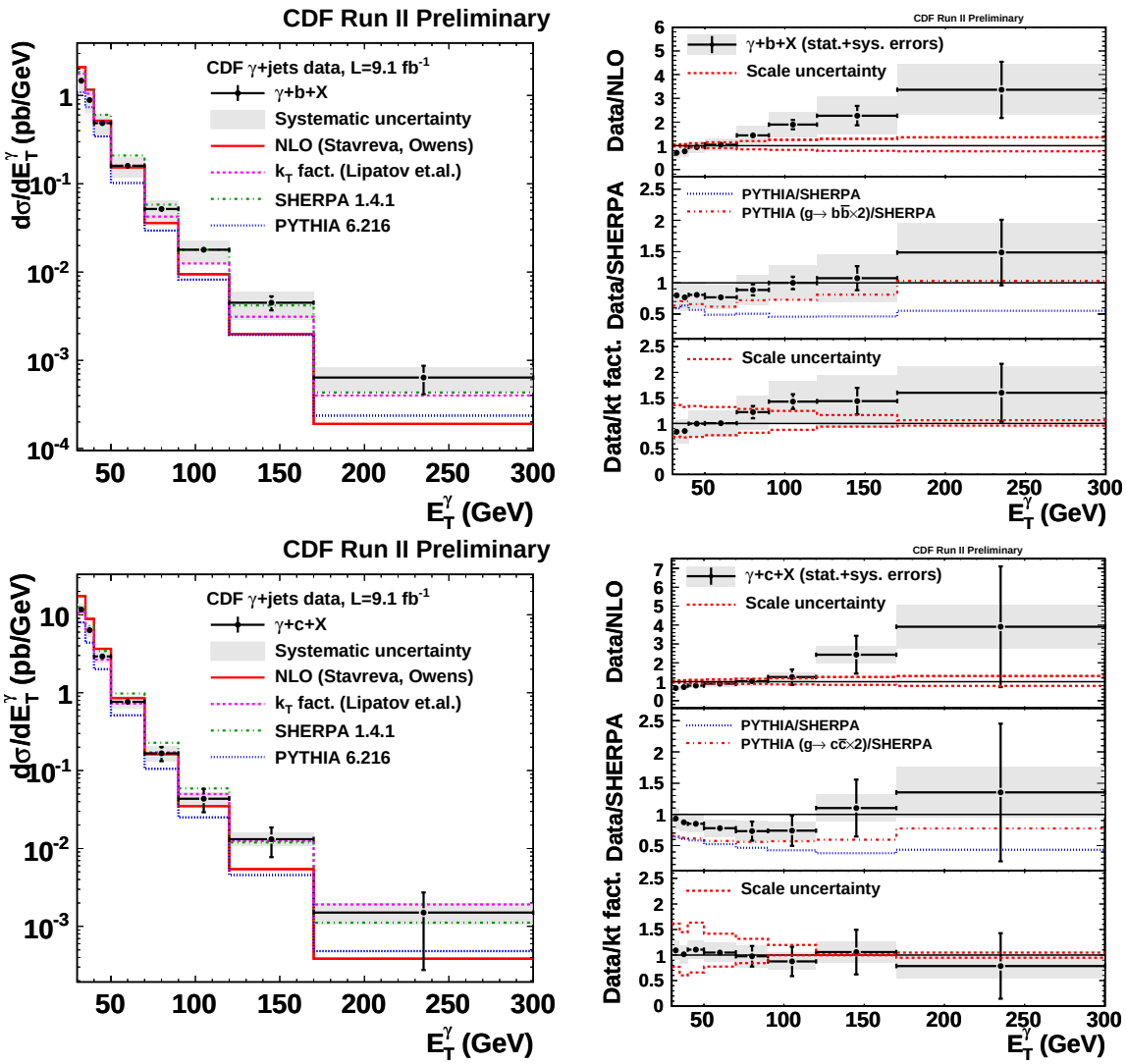

Figure 3: The measured differential cross sections compared with four theoretical predictions discussed in the text. The left windows show the absolute comparisons and the right windows show the ratios of the data over the theoretical predictions. The comparisons are shown for $\gamma + b + X$ (top) and $\gamma + c + X$ (bottom). The shaded area around the data points indicates the total systematic uncertainty of the measurement.

fusion and quark-(anti)quark interaction subprocesses, and the $\mathbf{k}_\mathrm{T}$-dependent (i.e. unintegrated) parton distributions, where $\mathbf{k}_\mathrm{T}$ denotes the transverse momentum of the parton. The k_T-factorization formalism incorporates effectively higher order contributions beyond NLO by resumming the gluon radiation in the $\mathbf{k}_\mathrm{T}^2$ region above the probing scale μ^2. The property of unintegrated parton distributions and the non-vanishing transverse momentum distribution of the colliding partons lead to a broadening of the photon transverse momentum distribution. The scale dependence is evaluated in the same way as the NLO calculation.

Both the NLO and k_T-factorization predictions are corrected for non-perturbative effects of parton-to-hadron fragmentation and underlying events using SHERPA Monte Carlo (MC) sample. The correction factors are shown in Table 1 for different E_T^γ bins.

We compare our measurements with predictions of SHERPA 1.4.1 MC generator [18] with CT10 PDFs in Table 1 and Fig. 3. This calculation includes all the matrix element (ME) diagrams with one photon and up to three jets, with at least one b-jet or c-jet in our kinematic region. This calculation features a parton-jets matching procedure to avoid overlapping between phase-space descriptions give by ME generators and showering/hadronization in multi-jets process simulation.

We also compare our measurements with predictions of PYTHIA 6.216 MC event generator [19] with CTEQ5L PDFs. This calculation includes the $2 \to 2$ ME subprocesses $gb \to \gamma b$ and $q\bar{q} \to \gamma g$ and, with $g \to b\bar{b}$ and $g \to c\bar{c}$ splittings in the parton shower (PS). It was shown in previous studies that the contribution of gluon splitting in heavy flavor had to be roughly doubled over expectations from the leading order PYTHIA MC generator [17]. In light of that, we show predictions after we increase the gluon splitting rates in heavy flavor quarks by a factor of two in Fig 3.

The NLO pQCD predictions agree with data at low E_T^γ but fail to describe data for $E_T^\gamma > 70$ GeV for bottom jet cross section, which indicates the need for higher order corrections in this calculation. The same trend is observed in the charm jet cross section even though the experimental uncertainty is considerably larger. The k_T-factorization and SHERPA predictions are in reasonable agreement with the measured cross sections within theoretical and experimental uncertainties. The PYTHIA predictions underestimate the measured cross sections in the entire kinematic range and the agreements deteriorate as E_T^γ goes up. After we double the rate of $g \to b\bar{b}$ or $g \to c\bar{c}$, the PYTHIA predictions agree better with the measured cross sections in shape.

In conclusion, we have measured the differential cross sections of inclusive production of photon in association with a heavy flavor quark using data corresponding to an integrated luminosity of 9.1 fb^{-1} collected by the CDF II detector at the Fermilab Tevatron. Our results indicate higher order corrections to the NLO pQCD predictions are necessary to describe our data. The k_T-factorization and SHERPA calculations describe data much better. The comparison to PYTHIA calculations confirms the need for a better understanding of gluon splitting rate in heavy flavors in this generator. These results can be used to improve the background modeling in the searches for new physics in channels involving the production of photons in association with heavy flavor quarks.

We are grateful to A. V. Lipatov, M. A. Malyshev, N. P. Zotov, F. Siegert, T. P. Stavreva and J. F. Owens for providing theoretical predictions and for many useful discussions. We thank the Fermilab staff and the technical staffs of the participating institutions for their vital contributions. This work was supported by the U.S. Department of Energy and National Science Foundation; the Italian Istituto Nazionale di Fisica Nucleare; the Ministry of Education, Culture, Sports, Science and Technology of Japan; the Natural Sciences and Engineering Research Council of Canada; the National Science Council of the Republic of China; the Swiss National Science Foundation; the A.P. Sloan Foundation; the Bundesministerium für Bildung und Forschung, Germany; the Korean World Class University Program, the National Research Foundation of Korea; the Science and Technology Facilities Council and the Royal Society, UK; the Russian Foundation for Basic Research; the Ministerio de Ciencia e Innovación, and Programa Consolider-Ingenio 2010, Spain; the Slovak R&D Agency; the Academy of Finland; and the Australian Research Council (ARC).

References

[1] T. P. Stavreva and J. F. Owens, Phys. Rev. D **79**, 054017 (2009).

[2] V. M. Abazov *et al.* (D0 Collaboration), Phys. Rev. Lett. **102**, 192002 (2009).

[3] S. J. Brodsky, arXiv:1202.5338.

[4] V. M. Abazov *et al.* (D0 Collaboration), Phys. Lett. B **714**, 32 (2012); V. M. Abazov *et al.* (D0 Collaboration), arXiv:1210.5033.

[5] T. Aaltonen *et al.* (CDF Collaboration), Phys. Rev. D **81**, 052006 (2010).

[6] A cylindrical coordinate system, (r, ϕ, z) is used with origin at the geometric center of the detector. r is the radius from the nominal beam line, ϕ is the azimuthal angle, and $+z$ points along the direction of the proton beam. The polar angle θ with respect to the proton beam defines the pseudorapidity η which is given by $\eta = -\ln[\tan(\theta/2)]$. Transverse energy and transverse momentum are defined as $E_T = E\sin(\theta)$ and $p_T = p\sin(\theta)$, respectively.

[7] A. Sill, Nucl. Instrum. Methods Phys. Res., Sec. A **447**, 1 (2000).

[8] T. Affolder *et al.*, Nucl. Instrum. Methods Phys. Res., Sec. A **526**, 249 (2004).

[9] L. Balka *et al.* (CDF Collaboration), Nucl. Instrum. Methods Phys. Res., Sec. A **267**, 272 (1988); S. Bertolucci *et al.* (CDF Collaboration), Nucl. Instrum. Methods Phys. Res., Sec. A **267**, 301 (1988); M. G. Albrow *et al.* (CDF Collaboration), Nucl. Instrum. Methods Phys. Res., Sec. A **480**, 524 (2002).

[10] G. Apollinari *et al.*, Nucl. Instrum. Methods Phys. Res., Sec. A **412**, 515 (1998).

[11] G. Ascoli *et al.*, Nucl. Instrum. Methods Phys. Res., Sec. A **268**, 41 (1988).

[12] T. Aaltonen *et al.* (CDF Collaboration), Phys. Rev. D **82**, 052005 (2010).

[13] T. Aaltonen *et al.* (CDF Collaboration), Phys. Rev. Lett. **108**, 011801 (2012).

[14] F. Abe *et al.* (CDF Collaboration), Phys. Rev. D **45**, 1448 (1992).

[15] A. Bhatti *et al.* (CDF Collaboration), Nucl. Instrum. Methods Phys. Res., Sec. A **566**, 375 (2006).

[16] D. Acosta *et al.* (CDF Collaboration), Phys. Rev. D **72**, 052003 (2005).

[17] B. Abbott *et al.* (D0 Collaboration), Phys. Lett. B **487**, 264 (2000); D. Acosta *et al.* (CDF Collaboration), Phys. Rev. D **71**, 092001 (2005); T. Aaltonen *et al.* (CDF Collaboration), Phys. Rev. D **78**, 072005 (2008).

[18] T. Gleisberg, S. .Hoeche, F. Krauss, M. Schonherr, S. Schumann, F. Siegert and J. Winter, J. High Energy Phys. **0902**, 007 (2009).

[19] T. Sjostrand, S. Mrenna and P. Z. Skands, J. High Energy Phys. **0605**, 026 (2006).

[20] S. P. Baranov, A. V. Lipatov and N. P. Zotov, Eur. Phys. J. C **56**, 371 (2008);

A. V. Lipatov, M. A. Malyshev and N. P. Zotov, J. High Energy Phys. **1205**, 104 (2012).